Biosensors and Bioelectronics 26 (2011) 4436–4441

Contents lists available at ScienceDirect

Biosensors and Bioelectronics

journal homepage: www.elsevier.com/locate/bios

A novel nitrite biosensor based on single-layer graphene nanoplatelet–protein composite film

Rong Yue, Qing Lu*, Yikai Zhou

MOE Key Lab of Environment and Health, School of Public Health, Tongji Medical College, Huazhong University of Science and Technology, Wuhan 430030, PR China

ARTICLE INFO

Article history:
Received 9 November 2010
Received in revised form 18 March 2011
Accepted 29 April 2011
Available online 6 May 2011

Keywords:
Biosensor
Direct electron transfer
Myoglobin
Nitrite determination
Single-layer graphene nanoplatelet

ABSTRACT

A novel nitrite biosensor was developed through a sensing platform consisted of single-layer graphene nanoplatelet (SLGnP)–protein composite film. SLGnP with the virtues of excellent biocompatibility, conductivity and high sensitivity to the local perturbations can provide a biocompatible microenvironment for protein immobilization and a suitable electron transfer distance between electroactive centers of heme protein and electrode surface. A pair of well-defined and quasi-reversible cyclic voltammetric peaks that reflected the direct electrochemistry for ferric/ferrous couple of myoglobin (Mb) was achieved at the composite film modified electrode. Field emission scanning electron microscopy (FESEM) and ultraviolet visible spectra (UV–vis) were utilized to characterize the composite film. The results demonstrated that the morphology of the composite film was unique and the protein in the composite film retained its secondary structure similar to the native state. The composite film also displayed excellent electrocatalytic ability for the reduction of nitric oxide, which was applied to determine nitrite indirectly. It exhibited good electrochemical response to nitrite with a linear range from 0.05 to 2.5 mM and a detection limit of 0.01 mM.

1. Introduction

Nowadays, nitrites are used in a large amount as preservatives and fertilizing agents. However, the continuous ingestion of these ions can be harmful for animal and human health (Kroupova et al., 2008; Deane and Woo, 2007; Rodrigues et al., 2007; Shailaja et al., 2006). For instance, nitrite in the bloodstream can cause the irreversible oxidation of hemoglobin to methemoglobin, which has no oxygen carrying ability. This conversion will reduce the oxygen-transporting capacity of blood, therefore may induce methemoglobinemia or "blue baby syndrome" (Bruningfann and Kaneene, 1993). Moreover, nitrite inside the body can react with amines to form carcinogenic nitrosamines and other N-nitroso compounds as well (Kroupova et al., 2008). Consequently, there is a growing demand for nitrite detection in food, drinking water and environmental samples.

Several analytical technologies have been described for nitrite determination, including spectrophotometry (Griess reaction), ionic chromatography polarography, capillary electrophoresis, and fluorescence spectrophotometric methods (Moorcroft et al., 2001). However, most of these conventional approaches are expensive and time-consuming. In addition to the above demerits, the utilization of conventional methods generates considerable waste and requires professional technician. Furthermore, these methods are not adequately capable of achieving real-time on-site measurement required for a strict environmental control. In this context, it is of importance and urgency to develop reliable alternative method for fast and in situ monitoring nitrite. In particular, biosensors can offer considerable promises for attaining the analytical information in a faster, simpler and cheaper manner compared with centralized analytical systems and constituting a field portable monitoring device (Thévenot et al., 2001). Nitrite determination has been previously achieved by enzymatic biosensors, which are usually based on the immobilization and electrical wiring of nitrite reductase (NiR) (Scharf et al., 1995; Strehlitz et al., 1996; Wu et al., 1997; Sasaki et al., 1998; Silva et al., 2004). However, the major obstacles of the NiR-based nitrite biosensors are the poor stability of the enzyme and the difficulty in establishing an electrical communication with the immobilized reductase.

The nitrite ion may disproportionate according to the following equation (Stanbury et al., 1989; Pan et al., 2001):

$$3NO_2^- + H_2O \leftrightarrows 2NO(aq) + NO_3^- + 2OH^-$$

Therefore, when nitrite ion exists in an acidic medium, the generation of nitric oxide (NO) is thermodynamically favorable. Nitric oxide has a high affinity with heme proteins by binding to heme-ferrous (heme-Fe(II)) (Gow and Stamler, 1998). The interactions between NO and heme proteins have a significant influence

* Corresponding author. Tel.: +86 27 83692333; fax: +86 27 83657765.
E-mail addresses: qiweiliao@gmail.com, qi_weiliao@126.com (Q. Lu).

0956-5663/$ – see front matter © 2011 Elsevier B.V. All rights reserved.
doi:10.1016/j.bios.2011.04.059

on the electrochemical responses of NO and proteins, which provides a good chance of achieving indirect determination of nitrite. The capability of the above hypothesis has been approved by the successful determinations of nitrite using biosensors based on hemoglobin (Hb) immobilized on carbon nanotube, silk fibroin and so on (Wu et al., 2006; Liu et al., 2007; Lu et al., 2007).

Nanomaterials are suitable for acting as "electronic wires" to shorten the electron transfer distance and enhance the electrical communications between redox centers of heme proteins and electrode surface (Zhao et al., 2008). Recently, graphene and graphene-based materials have emerged to be fascinating materials from perspectives of fundamental science and technology (Novoselov et al., 2004; Ponomarenko et al., 2008). These materials have the virtues of nontoxicity, chemical and thermal tolerance, electric conductivity and mechanical hardness, which promise wide range industrial applications in energy storage, catalyst support, structural and electronic components as well as in biotechnology (Geim and Novoselov, 2007; Novoselov et al., 2007). For example, single-layer graphene nanoplatelet (SLGnP) possesses extremely high electric sensitivity to local perturbations, such as surface charges and adsorbed gas molecules (Schedin et al., 2007; Martin et al., 2008). SLGnP also has many attractive features such as biocompatibility, high conductivity and large effective surface area. These characteristics are advantageous for its application in direct electrochemistry-based biosensors.

In this work, a novel nitrite biosensor is fabricated through the platform composed of SLGnP–heme protein composite film. Here, myoglobin (Mb), a type of heme protein, is selected as a model for analysis. Direct electron transfer of the protein is achieved at the composite film modified electrode. SLGnP is proved to be effective in providing a biocompatible microenvironment for protein immobilization and a suitable electron-transfer distance between the protein's electroactive centers and the electrode surface. The composite film also displays excellent electrocatalytic reduction ability for NO, which offers a practical approach for the indirect determination of nitrite subsequently.

2. Experimental

2.1. Reagents

Myoglobin (Mb, from equine skeletal muscle, MW 17,000) and tetrasodium 1,3,6,8-pyrenetetrasulfonic acid (TPA) were obtained from Sigma and used without further purification. Single-layer graphene nanoplatelet was prepared *via* a typical method as follows (Dong et al., 2009). 1 mg natural graphite flakes (NGS, Germany) were mixed with 10 mg TPA in 5 mL tri-distilled water. The mixture was then sonicated by a probe sonicator (pulse mode at 80 W) in an ice bath for 2 h. After gravity sedimentation over night and centrifugation, the resulting supernatant was taken as SLGnP–TPA. Sodium nitrite ($NaNO_2$, Shanghai Reagent Corporation, Shanghai, China) was dissolved in tri-distilled water to form 1 M stock solution. All other chemicals were of analytical grade. All solutions were prepared with tri-distilled water. Protein solution was stored in refrigerator at 4 °C prior to usage.

2.2. Preparation of the composite film modified electrode

A glassy carbon (GC) electrode was first polished with 0.3 and 0.05 μm alumina slurry, and then sonicated in nitric acid (1:1), ethanol and tri-distilled water in turn. Mb dissolved in tri-distilled water (10 mg/mL) was mixed with SLGnP–TPA in 1:1 (v/v) ratio. Then, 5 μL of the mixture was pipetted to the surface of the freshly prepared GC electrode. The electrode was dried at ambient temperature over night. Before electrochemical experiments, 1 μL Nafion (Aldrich, diluted to 0.5% with tri-distilled water) functioning as a binder to hold the composite film was cast onto the SLGnP–TPA–Mb film modified electrode. The solvent was allowed to evaporate and the final electrode is represented as Nafion/SLGnP–TPA–Mb/GC electrode.

2.3. Apparatus

Cyclic voltammetry (CV) was carried out at an EC550 electrochemical workstation (Gaoss Union Technology Co., Ltd., Wuhan, China). A three-electrode system was employed, including a working Nafion/SLGnP–TPA–Mb/GC electrode, a saturated calomel reference electrode (SCE) and a platinum wire counter electrode. Prior to each electrochemical experiment, the phosphate buffer solutions were purged with high-purity nitrogen for at least 30 min. A nitrogen environment was kept over the solutions in the cell during the experimental processes. All experiments were performed at room temperature. Ultraviolet visible spectroscopy (UV–vis) was recorded with a Lambda 35 UV–vis spectrophotometer (PE, USA). Field emission scanning electron microscopy (FESEM) images were measured with a Sirion 200 field-emission scanning electron microanalyzer (FEI, Netherlands). X-ray photoelectron spectroscopy (XPS) analysis was carried out by using a Thermo VG Multilab 2000 spectrometer (UK) with a monochromatic Al Kα source and a charge neutralizer. The characteristic spectra of C 1s, O 1s, N 1s, S 2p and Fe 2p of XPS were investigated and recorded. The samples for Mb and SLGnP–TPA were prepared by depositing Mb and SLGnP–TPA solutions onto glass slides with same concentration as for GC electrodes described above and then were dried in air overnight. The sample for the composite was prepared by immerging the glass slide covered with SLGnP–TPA into Mb solution (same concentration as above) for about 2 h, and then was dried in air overnight. For comparison, the bare glass slide was used as blank.

3. Results and discussion

3.1. Characteristics of the SLGnP–TPA–Mb composite film

Field emission scanning electron microscopy (FESEM) was used to characterize the morphology of the composite film. The surface morphologies of SLGnP–TPA, Mb and SLGnP–TPA–Mb films on a GC block are illustrated in Fig. 1. The protein film displays a flat but apertured structure (Fig. 1A), while the SLGnP–TPA film features aggregated acicular crystal clusters (Fig. 1B). Different from the morphologies above, the SLGnP–TPA–Mb composite film (Fig. 1C) demonstrates a homogeneous flake-like configuration. As shown in a high-magnification FESEM image (Fig. 1D), the flakes of the composite film stand in different directions, like petals, with the widths about 200 nm. The difference of the morphologies indicates strong interactions exist between the protein and SLGnP–TPA, which have an effect on the microstructure of the composite film. It is well known that the isoelectric point of Mb is 7.07. Therefore, the protein dissolved in tri-distilled water (acidulous) is positively charged. On the other hand, in view of the abundant sulfonic groups of TPA, SLGnP dispersed by TPA molecules is negatively charged. Accordingly, there exist electrostatic attractions between Mb and SLGnP–TPA due to the different charges they have. In order to testify whether the protein was attached to SLGnP–TPA, an X-ray photoelectron spectroscopy (XPS) study was carried out. The corresponding results were illustrated in Supporting Information. The XPS survey spectra of Mb (SI-1, A and B) demonstrated a typical N 1s peak at a binding energy of 399.3 eV, which could be assigned to peptide bonds (O=C–N–) of protein (Nho, 2003). Similar XPS spectra were obtained for the composite (SI-1, E and F). However, the

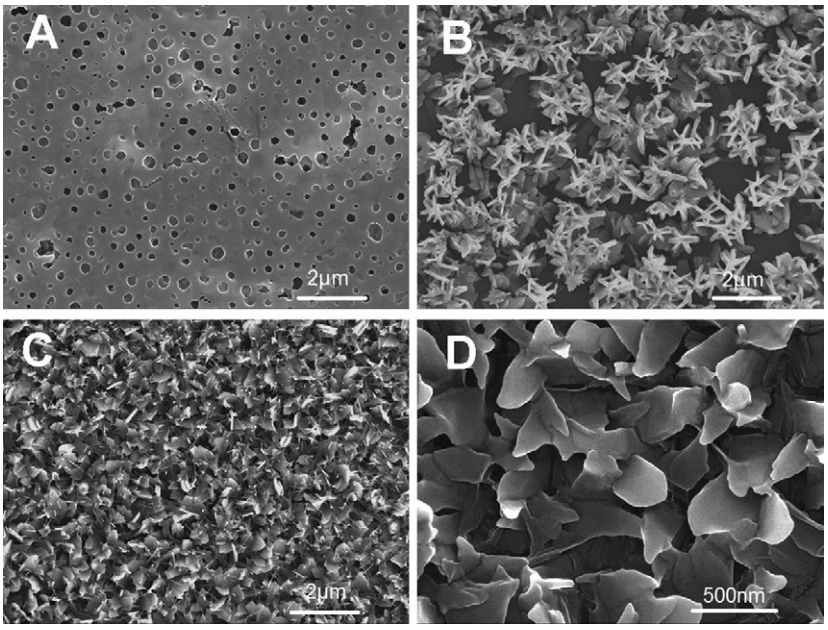

Fig. 1. Typical FESEM images with the same magnification of (A) Mb film, (B) SLGnP–TPA film and (C) SLGnP–TPA–Mb composite film at a GC block. Magnified FESEM image of (D) SLGnP–TPA–Mb composite film at a GC block.

XPS of SLGnP–TPA showed scarcely any N 1s peak (SI-1, C and D). The results suggested that the protein could attach to SLGnP–TPA due to the electrostatic interactions between them. The XPS data analysis was listed in SI-2.

Generally, the Soret absorption band of heme prosthetic group in heme proteins is sensitive to its microenvironment, substructure, and oxidation state. Thus, the shape and position of the Soret absorption band may provide additional information about possible denaturation of protein molecules, especially the conformational change in heme group region (Chi and Asher, 1998; Chi and Asher, 1999). Fig. 2 gives the UV–vis spectra of SLGnP–TPA–Mb, Mb and SLGnP–TPA solutions. For the SLGnP–TPA solution (curve c), two intensive absorption peaks are observed around 355 and 376 nm, respectively, which are characterized to the ultraviolet absorption of TPA (Liu et al., 1997). And for the SLGnP–TPA–Mb solution (curve a), besides the same peaks derived from TPA, a broad absorption peak appears at 406 nm, which is virtually identical to the Soret absorption band of the native Mb solution (curve b). The results from UV–vis spectra indicate the protein can retain its natural structure in the composite, which is particularly critical to keep the protein's functions in the incorporated film.

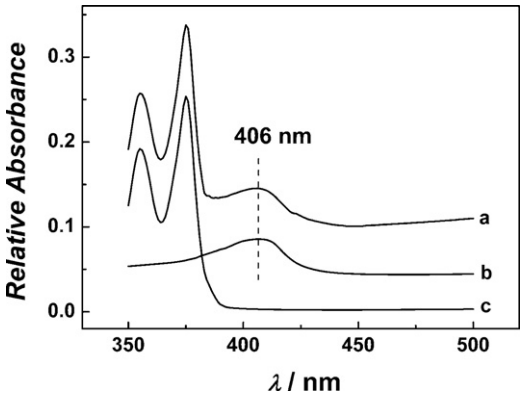

Fig. 2. UV–vis spectra of (a) SLGnP–TPA–Mb, (b) Mb, (c) SLGnP–TPA solutions. The absorbance coordinate only reflects relative absorbance.

3.2. Electrochemical characteristics of the SLGnP–TPA–Mb composite film

Same as other nanomaterials, SLGnP as an immobilizing material for Mb can act as "electronic wires" to shorten the electron transfer distance and enhance the electrical communications between redox center of the heme protein and the electrode surface. The electrochemical behavior was analyzed by cyclic voltammetry (CV). It is worth mentioning here, the SLGnP–TPA–Mb composite film was very easy to peel off from the surface of GC electrode during the process of CV scans. Thus, it is hard to obtain stable electrochemical behaviors of the SLGnP–TPA–Mb film modified GC electrode. In order to overcome this problem, Nafion was cast onto the composite film and used as a binder. Nafion utilized here had a very low concentration (0.5%). It only partially covered the composite film and was not involved in any electrochemical reactions. The corresponding CV results are presented in Fig. 3. Obviously, a pair of well-defined and quasi-reversible redox peaks appears at the CV of Nafion/SLGnP–TPA–Mb film modified GC electrode (curve a).

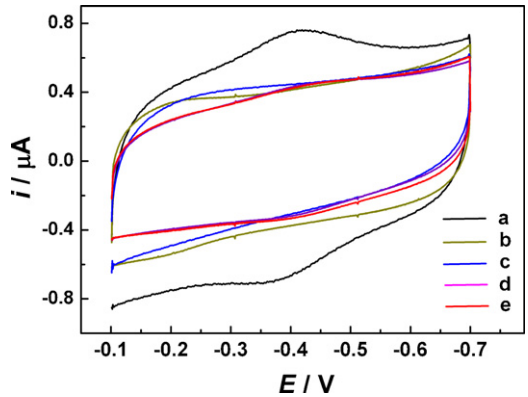

Fig. 3. Cyclic voltammograms at 0.1 V s^{-1} in pH 7.4 buffers for (a) Nafion/SLGnP–TPA–Mb film (dark), (b) Nafion/SLGnP–TPA film (dark yellow), (c) the bare GC electrode (blue), (d) Nafion/Mb film (magenta) and (e) Nafion/TPA–Mb film (red). (For interpretation of the references to colour in this figure legend, the reader is referred to the web version of the article.)

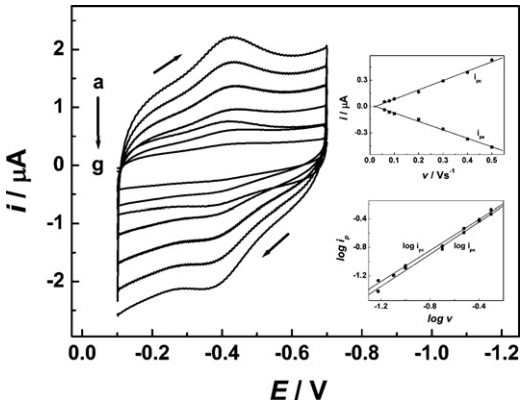

Fig. 4. Cyclic voltammograms at $0.1\,V\,s^{-1}$ in pH 7.4 buffers for Nafion/SLGnP–TPA–Mb film at scan rates of (a) 0.5, (b) 0.4, (c) 0.3, (d) 0.2, (e) 0.1, (f) 0.08, (g) $0.06\,V\,s^{-1}$. The inset are plots of the reduction and oxidation peak current i against the scan rate ν (upper) and the logarithm of i against the logarithm of ν (lower).

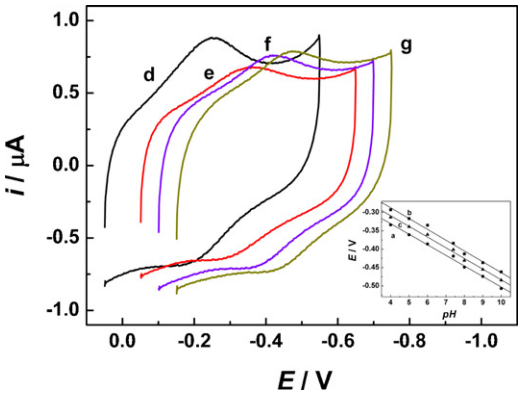

Fig. 5. Cyclic voltammograms at $0.1\,V\,s^{-1}$ for Nafion/SLGnP–TPA–Mb film in phosphate buffer solutions of pH (d) 3.0, (e) 5.0, (f) 7.4, (g) 9.0. The inset shows the relationship between (a) E_{pc}, (b) E_{pa}, (c) $E^{\circ\prime}$ of Nafion/SLGnP–TPA–Mb film and the solution pH value.

However, there is no redox peak observed at the bare GC electrode (curve c) and the Nafion/SLGnP–TPA film modified GC electrode (curve b). The phenomena above indicate that the pair of redox peaks in curve a is the characteristic of electroactive centers of Mb. Curves d and e in Fig. 3 also display the relatively featureless cyclic voltammograms of Nafion/Mb and Nafion/TPA–Mb films, respectively. This indicates Nafion and TPA have little contributions to the enhancement for the direct electron transfer of the protein. The phenomena also suggest that SLGnP plays an essential role in enhancing the direct electron transfer of the heme protein. In curve a, the anodic peak potential (E_{pa}) and the cathodic peak potential (E_{pc}) are located at about −0.385 V and −0.419 V, respectively, with a formal potential ($E^{\circ\prime}$, defined as the average of E_{pa} and E_{pc}) at −0.402 V. The separation of the peak potential (ΔE_p) is 34 mV, in excess of the ideal thin-film value of 0 mV (Murray, 1984), which means the electrochemical reaction of Mb is a quasi-reversible thin-film electrochemical reaction. All these values coincide well with the behavior of the direct electrochemistry of heme Fe(III)/Fe(II) couples of the proteins (Onuoha and Rusling, 1995; Chen and Tseng, 2005). In addition, the ΔE_p value for SLGnP–TPA–Mb film is much smaller than that of Mb-CNTs reported in the literature (Zhang et al., 2004), indicating the better direct electron-transfer enhancement of SLGnP, which ascribes to the unique characteristics of graphene.

The effect of the scan rate on the electrochemical response of the SLGnP–TPA–Mb composite film was also investigated by CV, as shown in Fig. 4. It is obvious that the redox peak currents enlarge gradually with the increase of the scan rate. The reduction and oxidation peak currents of the composite film are linearly proportional to the scan rate in the range from 0.06 to $0.5\,V\,s^{-1}$ (Fig. 4, upper inset). The coulombic charge (Q), obtained by integrating the currents of anodic or cathodic peak in CVs against time, is nearly constant and independent of scan rates in the same range. In addition, both the $\log i_{pc} - \log \nu$ and $\log i_{pa} - \log \nu$ plots illustrate linear relationship (Fig. 4, lower inset), with the ratio of the slopes about one. All these results suggest that the electrochemical reaction of the composite film is a typical surface-confined or thin-layer electrochemical behavior (Rusling and Nassar, 1993). During this process, all electroactive ferrous proteins (protein-Fe(II)), which are produced by the reduction of ferric proteins (protein-Fe(III)) on the cathodic scan, can be oxidized to protein-Fe(III) on the anodic scan. The apparent heterogeneous electron transfer rate constant k_s of Mb in SLGnP–TPA film can be estimated to be $3.9\,s^{-1}$ by using the equation derived by Laviron for diffusionless CV (Laviron, 1979). It indicates SLGnP–TPA is an excellent promoter for the electron transfer between the protein and the electrode.

The change of pH value of the external solution can modulate the accessibility of water to the heme pocket of heme-protein and the protonation of the heme ironbound proximal histidine and/or the distal histidine in the heme pocket. Fig. 5 displays that the pH value of external solution has a strong influence on the redox potentials of the SLGnP–TPA–Mb film. It is exhibited that with the increase of the solution pH value, both E_{pa} and E_{pc} shift to a negative direction. It suggests a proton-transfer involved redox reaction. An asymmetric redox CV is observed when the pH is fixed to be 3.0 (curve d). Subsequently, a normal well-defined CV could be obtained when the same modified electrode was put back to the phosphate buffer solution of pH 7.4 (not shown). This phenomenon is likely due to a reversible pH-induced conformational change of Mb at low pH. Within the pH range between 4.0 and 10.0, E_{pa}, E_{pc} and $E^{\circ\prime}$ are dependent on the solution pH linearly with the slopes of about −29 mV/pH (Fig. 5, inset). The slope value is much smaller than the theoretical value (−59 mV/pH) for a single-proton coupled, reversible one-electron transfer (Yamazaki, 1978). The derivation of the slope may originate from the influence of the protonation of the water molecule coordinated to the heme-iron, or the protonation states of *trans* ligands to the heme iron and amino acids around the heme group (Kamin and Willson, 1980).

3.3. Electrocatalytic properties of the SLGnP–TPA–Mb composite film

It is well known that proteins and enzymes containing heme, such as hemoglobin, Mb and horseradish peroxidase have the ability to catalyze the reduction of NO and H_2O_2 (Spiro and Jarzecki, 2001). When nitrite exists in an acidic medium, a disproportionation reaction can take place with the generation of nitric oxide (Stanbury et al., 1989; Pan et al., 2001). Accordingly, the indirect electrochemical response for nitrite at the composite film modified electrode was investigated (illustrated in Fig. 6). Curve c in Fig. 6 is the cyclic voltammogram of the Nafion/SLGnP–TPA–Mb film modified GC electrode in pH 5.0 phosphate buffer solution. Only a pair of redox peaks at approximately −0.40 V is observed. When $NaNO_2$ is added into the solution, a cathodic peak at −0.77 V appears (curve d), and the peak current increases with the further addition of $NaNO_2$ (curve e). Meanwhile, the reduction and oxidation peak currents of the heme Fe(III)/Fe(II) redox couple for Mb decrease. In blank experiments, no cathodic peak is obtained at the Nafion/SLGnP–TPA electrode without (curve a) or with 0.3 M $NaNO_2$ (curve b). However, when the phosphate buffer solution was changed to neutral, the cathodic peak located at −0.77 V did not appear at the CV of Nafion/SLGnP–TPA–Mb film modified GC

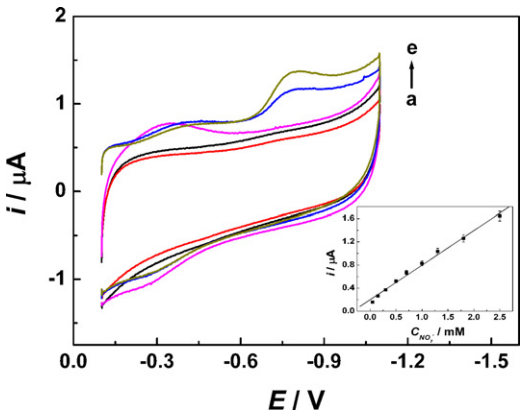

Fig. 6. Cyclic voltammograms at 0.1 V s^{-1} in pH 5.0 buffer for (a) Nafion/SLGnP–TPA and (c) Nafion/SLGnP–TPA–Mb films in buffer without $NaNO_2$, (b) Nafion/SLGnP–TPA and (d) Nafion/SLGnP–TPA–Mb films in buffer containing 0.3 mM $NaNO_2$, (e) Nafion/SLGnP–TPA–Mb film in buffer containing 0.7 mM $NaNO_2$. The inset is the plot of catalytic peak current *vs* the concentration of $NaNO_2$.

electrode with the addition of 0.3 M $NaNO_2$ (not shown). It may originate from the failure of generation of nitric oxide in the solution lack of proton ion. The results above confirm that the obtained cathodic peak is ascribed to the reduction of nitric oxide catalyzed by Mb. The mechanisms of the electrocatalytical reduction of nitric oxide at the Nafion/SLGnP–TPA–Mb film can be proposed as follows (Bayachou et al., 1998):

$$\mathrm{MbFe(III)} + \mathrm{e} \rightarrow \mathrm{MbFe\,(II)}$$

$$\mathrm{MbFe(II)} + \mathrm{NO} \rightarrow \mathrm{MbFe\,(II){-}NO}$$

$$\mathrm{MbFe(II){-}NO} + 2\mathrm{e} + 2\mathrm{H^+} \rightarrow \mathrm{MbFe\,(II)} + \mathrm{H_2O} + \mathrm{N_2O}$$

The cathodic peak current has a linear relationship with the concentration of NO_2^- in the range between 0.05 mM and 2.5 mM, as shown in the inset of Fig. 6, which indicates the Nafion/SLGnP–TPA–Mb film modified GC electrode can be used to fabricate an amperometric sensor for the detection of nitrite. And the linear regression equation is $I/\mu A = 0.198 + 0.598\,C/mM$, with a correlation coefficient 0.996 ($n = 9$). The sensitivity is calculated to be $3.42 \times 10^4\ \mu A\,M^{-1}\,cm^{-2}$. The detection limit is estimated to be 0.01 mM at a signal-to-noise ratio of 3. Compared with other systems, such as 0.233 mM for Hb-silk fibroin film and 0.286 mM for Hb/CTAB (Wu et al., 2006; Lu et al., 2007), this is a competitive value.

The stability of the Nafion/SLGnP–TPA–Mb/GC electrode was also studied. The CV currents could be remained at constant values upon 200 continuous CV cycles at the potential range from −0.1 to −1.2 V in pH 5.0 phosphate buffer solutions with the scan rate of 0.1 V s^{-1}. When the modified electrode was stored at 4 °C for about 2 weeks, it retained about 90% of its initial sensitivity to nitrite. The relative standard deviation (RSD) of the biosensor's response to 0.1 mM NO_2^- was 4.1% for eight successive measurements. The electrochemical responses of six electrodes, made simultaneously from the same resources, show an acceptable reproducibility with RSD of 5.2% for the current determined at 0.1 mM NO_2^-. The influence of uric acid, one of the main interferences in a biological fluid, was investigated for the detection of nitrite. No influence on the current response was observed in pH 5.0 buffer containing 0.2 mM NO_2^- with addition of uric acid more concentrated than NO_2^- by 10 times.

4. Conclusions

In summary, a new type nitrite biosensor was fabricated with the utilization of the SLGnP–TPA–Mb composite film. The virtues possessed by SLGnP, such as excellent biocompatibility, super conductivity and high sensitivity to the local perturbations, offer this novel nanomaterial promising application in direct electrochemistry-based biosensors. The composite film made up of SLGnP and Mb showed good electrochemical response to nitrite with the linear range of 0.05–2.5 mM and the detection limit of 0.01 mM. The fabricated nitrite biosensor exhibited high sensitivity and good stability.

Acknowledgements

The financial supports from National Basic Research Program of China (973 Program, No. 2009CB320301), National Natural Science Foundation of China (30901198) and Major Projects on Control and Rectification of Water Body Pollution (No. 2009ZX07527-007) are greatly acknowledged. The Center of Analysis and Testing of Huazhong University of Science and Technology is thanked for its help in FESEM observation.

Appendix A. Supplementary data

Supplementary data associated with this article can be found, in the online version, at doi:10.1016/j.bios.2011.04.059.

References

Bayachou, M., Lin, R., Cho, W., Farmer, P.J., 1998. J. Am. Chem. Soc. 120, 9888–9893.
Bruningfann, C.S., Kaneene, J.B., 1993. Vet. Human Toxicol. 35, 237–253.
Chen, S.M., Tseng, C.C., 2005. J. Electroanal. Chem. 575, 147–160.
Chi, Z., Asher, S.A., 1998. Biochemistry 37, 2865–2872.
Chi, Z., Asher, S.A., 1999. Biochemistry 38, 8196–8203.
Deane, E.E., Woo, N.Y.S., 2007. Aquatic. Toxicol. 82, 85–93.
Dong, X.C., Shi, Y.M., Zhao, Y., Chen, D.M., Ye, J., Yao, Y.G., Gao, F., Ni, Z.H., Yu, T., Shen, Z.X., Huang, Y.X., Chen, P., Li, L.J., 2009. Phys. Rev. Lett. 102, 135501.
Geim, A.K., Novoselov, K.S., 2007. Nat. Mater. 6, 183–191.
Gow, A.J., Stamler, J.S., 1998. Nature 391, 169–173.
Kamin, R.A., Willson, G.S., 1980. Anal. Chem. 52, 1198–1205.
Kroupova, H., Machova, J., Piackova, V., Blahova, J., Dobsikova, R., Novotny, L., Svobodova, Z., 2008. Ecotoxicol. Environ. Saf. 71, 813–820.
Laviron, E., 1979. J. Electroanal. Chem. 101, 19–28.
Liu, S.Q., Lin, B.P., Yang, X.D., Zhang, Q.Q., 2007. J. Phys. Chem. B 111, 1182–1188.
Liu, Z., Peng, J., Li, W., 1997. Chin. J. Lumin. 18, 161–165.
Lu, Q., Hu, C., Cui, R., Hu, S., 2007. J. Phys. Chem. B 111, 9808–9813.
Martin, J., Akerman, N., Ulbricht, G., Lohmann, T., Smet, J.H., Klitzing, K.V., Yacoby, A., 2008. Nat. Phys. 4, 144–148.
Moorcroft, M.J., Davis, J., Compton, R.G., 2001. Talanta 54, 785–803.
Murray, R.W., 1984. In: Bard, A.J. (Ed.), Electroanalytical Chemistry. Marcel-Dekker, New York.
Nho, Y.C., Kwon, O.H., 2003. Radiat. Phys. Chem. 66, 299–307.
Novoselov, K.S., Geim, A.K., Morozov, S.V., Jiang, D., Zhang, Y., Dubonos, S.V., Grigorieva, I.V., Firsov, A.A., 2004. Science 306, 666–669.
Novoselov, K.S., Jiang, Z., Zhang, Y., Morozov, S.V., Stormer, H.L., Zeitler, U., Maan, J.C., Boebinger, G.S., Kim, P., Geim, A.K., 2007. Science 315, 1379.
Onuoha, A.C., Rusling, J.F., 1995. Lagmuir 11, 3296–3301.
Pan, K.C., Chuang, C.S., Cheng, S.H., Su, Y.O., 2001. J. Electroanal. Chem. 501, 160–165.
Ponomarenko, L.A., Schedin, F., Katsnelson, M.I., Yang, R., Hill, E.W., Novoselov, K.S., Geim, A.K., 2008. Science 320, 356–358.
Rodrigues, R., Schwarz, M.H., Delbos, B.C., Sampaio, L.A., 2007. Aquaculture 271, 553–557.
Rusling, J.F., Nassar, A.E.F., 1993. J. Am. Chem. Soc. 115, 11891–11897.
Sasaki, S., Karube, I., Hirota, N., Arikawa, Y., Nishihiyama, M., Kukimoto, M., Horinouchi, S., Beppu, T., 1998. Biosens. Bioelectron. 13, 1–5.
Scharf, M., Moreno, C., Costa, C., Vandijk, C., Payne, W.J., Gall, J.L., Moura, I., Moura, J.J.G., 1995. Biochem. Biophys. Res. Commun. 209, 1018–1025.
Schedin, F., Geim, A.K., Morozov, S.V., Hill, E.W., Blake, P., Katsnelson, M.I., Novoselov, K.S., 2007. Nat. Mater. 6, 652–655.
Shailaja, S., Rajamanickam, R., Wahidulla, S., 2006. Environ. Pollut. 143, 174.
Silva, S.D., Cosnier, S., Almeida, M.G., Moura, J.J.G., 2004. Electrochem. Commun. 6, 404–408.
Spiro, T.G., Jarzecki, A.A., 2001. Curr. Opin. Chem. Biol. 5, 715–723.
Stanbury, D.M., DeMaine, M.M., Doodloe, G., 1989. J. Am. Chem. Soc. 111, 5496–5498.
Strehlitz, B., Greundig, G., Schumacher, W., Kroneck, P.M.H., Vorlop, K.D., Kotte, H., 1996. Anal. Chem. 68, 807–816.

Thévenot, D.R., Toth, K., Durst, R.A., Wilson, G.S., 2001. Biosens. Bioelectron. 16, 121–131.
Wu, Q., Storrier, G.D., Pariente, F., Wang, Y., Shapleigh, J.P., Abruna, H.D., 1997. Anal. Chem. 69, 4856–4863.
Wu, Y., Shen, Q., Hu, S., 2006. Anal. Chim. Acta 558, 179–186.
Yamazaki, I., Araiso, T., Hayashi, Y., Yamada, H., Makino, R., 1978. Adv. Biophys. 11, 249–281.
Zhang, L., Zhao, G.C., Wei, X.W., Yang, Z.S., 2004. Chem. Lett. 33, 86–87.
Zhao, X., Mai, Z., Kang, X., Zou, X., 2008. Biosens. Bioelectron. 23, 1032–1038.